International Journal of Composite Materials 2017, 7(1): 20-36
DOI: 10.5923/j.cmaterials.20170701.03

Low-Velocity Impact Response and Damage Mechanism of 3D Fiber-Metal Laminates Reinforced with Amino-Functionalized Graphene Nanoplatelets

Zohreh Asaee, Mbarka Mohamed, Davide De Cicco, Farid Taheri*

Advanced Composite and Mechanics Laboratory, Department of Mechanical Engineering, Dalhousie University, Canada

Abstract The low-velocity impact response of graphene nanoplatelets (GNP) reinforced 3D fiber metal laminates (3DFML) is experimentally investigated. Two types of GNPs, pristine GNP (PG) and amino-functionalized GNP (NH2-G), are used strategically to reinforce the resin used to mate the two main constituents of the 3DFMLs. In order to establish the most optimal GNP content with respect to the impact response of 3DFML, three different weight-percentages of GNPs are considered and the responses are compared against that of the baseline specimens. The seven groups of specimens are subjected to three different impact energies. The results reveal that 1 wt% NH2-G is the optimal content, which could generate the greatest enhancement in resistance of the hybrid composite against impact, and minimizing the damage extent in the 3DFMLs. The study provides an in-depth analysis of force- and displacement-time history curves, force-displacement response, energy absorption capacity and damage mechanisms of the affected areas for all four groups of specimens.

Keywords Fiber-metal laminate, Nanoparticles, Low-velocity impact, 3D fabric, Graphene nanoplatelets, Functionalized nanoparticles

1. Introduction

Three-dimensional Fiberglass/Metal Laminates (3DFMLs) are a recently developed class of Fiber Metal Laminates (FML), consisting of 3D Fiber-Glass Fabric (3DFGF) and sheets of magnesium or other types of light-weight metallic alloys. Therefore, the major difference between this new FML and its traditional counterparts is in the use of a recently developed truly 3D E-glass fabric. When combined with a suitable polymeric resin, this new 3DFGF enables the FML to offer significantly more enhanced mechanical response in comparisons to the traditional FMLs made of 2D fabrics. Attributes such as superior specific bending stiffness and strength, light weight, high energy-absorption capacity under impact loadings, excellent thermal insulation and acoustic damping are some of the positive advantages of this new FML. The superior performance of this new bread of FML makes them suitable for applications in automotive, aerospace, marine and other weight-sensitive engineering applications [1].

The first generation of 2D FMLs were developed by researchers at the Delft University in the early 1980s [2-5]. The main attributes and advantages of the FMLs were noted as high specific strength and stiffness, better tolerance to fatigue crack growth, and good formability [6]. Since then, various categories of FMLs have been formed and marketed, which are distinguished based on the type of metal, and type and configuration of fibers/cloths used to form them. Moreover, because of their relatively superior damage tolerant attributes, many researchers have explored and investigated the response of those FMLs under low-velocity impact (LVI) [7-22].

In parallel, many researchers have also explored the possibility of gaining improvement in performance of fiber-reinforced plastic composites (FRPs) under LVI by addition of nanoparticles to the resins used to form FRPs [23-29]. For instance, Soliman et. al. [30] considered the LVI response of thin woven carbon fabric reinforced epoxy FRP. The investigated epoxy resin contained functionalized multi-walled carbon nanotubes (MWCNTs). Three different weight percentages of MWCNTs were considered: 0.5 wt%, 1 wt% and 1.5 wt%. The impact tests were performed at five levels of energy. The impact responses of tested composites and resulting damage mechanisms were examined and compared for each percentage of MWCNTs. The addition of functionalized MWCNTs was observed to have improved the impact response of the tested FRPs, and also limiting the extent of damage in the impacted specimens. A significant improvement in energy-absorption (approximately 50%) was attained when the resin contained only 1.5 wt% MWCNTs. In another study, Lin et al. [31] performed LVI

* Corresponding author:
farid.taheri@dal.ca (Farid Taheri)
Published online at http://journal.sapub.org/cmaterials

tests on an epoxy reinforced with various nanoparticles. Two types of nanoparticles (i.e., titanium dioxide and cloisite 30B) were used. Two to 10% nanoparticle volume contents were considered in their investigation. The results showed that the addition of the nanoparticles improved the performance of the resin markedly. Particle exfoliation and uniformity in particle dispersion significantly affected the response. Moreover, it was shown that the tensile strength, loss modulus, impact strength and dynamic thermal rheology of nanocomposites were all highly affected by the geometry, temperature, volume and type of filler content, and uniformity in the dispersion of the nanoparticles.

In another study, Haq et al. [26] studied the low-velocity impact response of sandwich composites comprising of glass fiber sheets and PVC foam with nano-graphene platelets (GNP) dispersed in the external layers of face sheets. The results of LVI tests of GNP doped specimens were compared with the pristine (i.e., with no GNP) specimens to investigate the influence of GNP on the impact response and damage extent in the specimens. They observed their GNP-doped specimens could absorb a greater amount of energy and exhibiting less damage extent in comparison to the pristine specimens.

2. Motivations and Objectives

The 3D fiber metal laminates introduced in this work, as illustrated in Figure 1, consist of a foam-filled truly 3D E-glass fabric, sandwiched between magnesium alloy (MgA) sheets. As explained in the previous works of authors [32-35], this 3DFML and its other configurations were developed with the aim of utilization as body panels in passenger and other transport vehicles. These 3DFMLs exhibit different damage mechanisms when compared to the conventional FMLs. The most significant difference is that in these panels, delamination occurs only at metal/3DFGF interfaces, with no delamination occurring within the fabric. As a result, FMLs made of 3DFGFs produce significantly greater energy-absorption capacity in comparison to their conventional 2D FML counterparts.

The main goal of this study is, therefore, to enhance the interface bond strength of these 3DFMLs cost-effectively, so to further improve their performance by mitigating the potential interface delamination. For that, the epoxy resin used for bonding the metal sheets to 3DFGF is reinforced with relatively inexpensive graphene nanoplatelets (GNPs). GNPs were selected as an effective reinforcement because of their superior mechanical properties and significantly lower cost compared to the other forms of nanocarbons (i.e., carbon-nanotubes, multi-walled carbon-nanotubes and Nano-carbon fibers). Moreover, Ahmadi-Moghadam et al. [36] demonstrated that functionalization of GNP nanoparticles significantly improved the nanoparticles/ epoxy matrix interface strength. They examined three different functionalization techniques on their GNPs (i.e., graphene oxide [GO], silane modified GNPs (G-Si) and amino functionalized GNP [NH2-G]), and compared the results with those obtained from the pristine GNPs. Their results showed that G-Si and NH2-G functionalized GNPs provided the most efficient improvement in the mechanical properties of their GNP-reinforced epoxy composites. Thus, the NH2-functionalized GNP is considered for investigation in this study. Therefore, the impact response of 3DFML panels formed by resin reinforced with pristine and NH2-functionalized GNPs will be investigated and compared to the response of 3DFML panels formed by neat epoxy. In addition, in order to establish the optimal GNP content for gaining the maximum enhancement in LVI response of 3DFMLs and mitigating the extent of their damage, three different weight contents (wt%) of GNPs are considered in this investigation (i.e., 0.5, 1 and 2 wt%).

3. Experimental Investigation

3.1. Materials

As stated earlier, GNP-reinforced 3DFMLs (referred to as GNP-3DFML hereafter), were manufactured from thin (0.5 mm) sheets of AZ31B-H24 MgA and the 3D E-glass fabrics. The sheets were acquired through the Metalmart International (Commerce, CA). The 3DFGF was acquired through China Beihai Fiberglass, Co. Ltd. (Jiujiang City, China). The fabric was wetted by an epoxy resin. Araldite LY 1564 (Bisphenole-A) resin with its hardener, Aradur 2954 (cycloaliphatic polyamine), supplied by the Huntsman Co. (West Point, GA) were used. The resin is a low viscosity and warm curing epoxy resin. The mixing ratio was 100:35 parts by weight as recommends by vendor. To further enhance the mechanical performance of the 3DFGF-reinforced epoxy composite, an 8-lb polyurethane foam (US Composites, West Palm Beach, FL 33407) was used to fill the hollow cores of the fabric (see Figure 1). This composite was then sandwiched in between two sheets of magnesium alloy. The resin used to mate the 3DFGF and magnesium sheets was mixed by pristine GNP nanoparticles obtained from XG Science (Lansing, MI). The average thickness, t, and average particle diameter, D, of GNP was 7 nm and 25 μm, respectively (See Figure 2). Amino-functionalized GNP (NH2-G), with an average diameter of 8 μm and average thickness of 5 nm were provided through Cheap Tubes Inc. (Brattleboro, VT). The mechanical properties of the 3DFGF, magnesium sheet, epoxy resin, polyurethane foam and GNP are presented in Table 1.

Table 1. Properties of the materials

3D Fiberglass Woven Fabrics	Weight per unit area = 800 g/m^2, Core Thickness = 4 mm
Magnesium AZ31B-H24	Thickness = 0.5 mm Modulus of Elasticity = 45 GPa, Ultimate Tensile Strength = 290 MPa, Tensile Yield Strength = 220 MPa Compressive Yield Strength = 180 MPa
Polyurethane Foam	Density = 128 kg/m^3, Expansion Rate = Approx. 8x liquid volume, Compressive Strength = 1.72 MPa Tensile Strength = 1.55 MPa Shear Strength = 0.89 MPa Flexural Strength = 2.40 MPa.

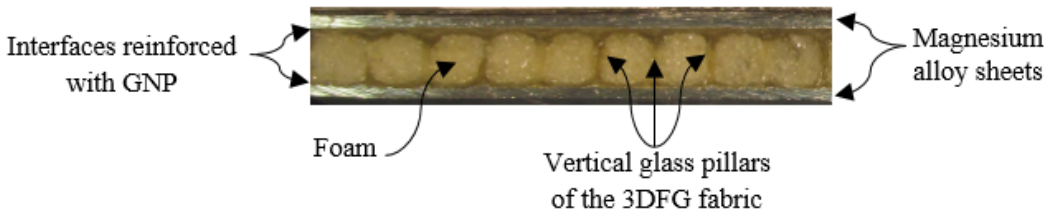

Figure 1. The detail of the GNP- reinforced 3D fiber metal laminate (GNP-3DFML)

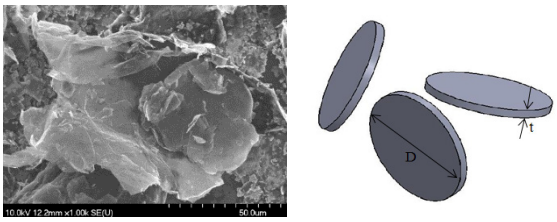

(a) (b)

Figure 2. (a) SEM image of typical GNPs used in this study, and (b) their idiazied schematic [37]

3.2. Procedures

In the first stage, the epoxy resin and its hardener were mixed using an electric paddle mixer at 100 rpm for 10 min, and then degassed in a vacuum chamber at room temperature for an hour. Afterwards, the mixture was applied onto the 3DFGF and cured in an oven for two hours at 60°C and eight hours at 120°C, per the manufacture instructions. Then, the two-parts polyurethane foam were mixed and injected by a syringe into the hollow cores of the foam.

As stated, the resin used to mate the cured 3DFGFand magnesium sheets was reinforced with pristine and NH2-functionalized GNPs. For that, the same epoxy used for fabricating the 3DFGF, was reinforced by the two types of GNP particles. The GNP particles were first thoroughly mixed into the resin using the electric paddle mixer at 1000 rpm for 15 min. Afterwards, the GNP-resin slurry was passed through a three-roll mill (Torrey Hill Technology, San Diego, CA) to uniformly disperse the GNP particles following the optimized procedure outline in reference [37]. Subsequently, the hardener was added to the GNP-resin mixture and degassed in a vacuum chamber at room temperature. The mixture was then used to adhere the cured 3DFGF and two magnesium sheets. Before doing so, the bonding surfaces of Mg sheets were first sand-blasted with 20/40 grit sand and the sanded surfaces were cleaned with compressed air, and then wiped clean with acetone. The GNP-epoxy mixture was applied to both mating surfaces, and the 3DFML assembly were vacuum-bagged and let cure for two hours at 60°C, and then for eight hours at 120°C.

3.3. Testing Procedure

A total of 63 specimens were fabricated and categorized into seven groups based on the GNP type (pristine GNP (PG) and NH2-funtionalized GNP (NH2-G)), and their weight content (see Table 2). The specimens were then subjected to three different levels of impact energies. The energy levels were selected based on our previous investigations [34]. The specifics of the tested specimens are presented in Table 2.

The impact tests in this study were conducted using a modified Charpy impact test equipment as illustrated in Figure 3. The equipment consists of a swinging pendulum, equipped with a contact mass, which can be changed to a specific mass as desired, and an impactor. Therefore, the impact energy and velocity can be varied by changing the mass and initial resting angle of the pendulum. The impactor sits within a specially designed guiding housing, containing bearings that guide and facilitate smooth and precise travel of the impactor on a single axis.

Each specimen was held (sandwiched) between two thick square steel plates, each with a 60 mm diameter hole in the center, clamped along the edges (see Figure 3(b)). Each specimen was impacted by a hemispherical profiled impactor with 16 mm diameter, also shown in Figure 3(b).

Table 2. Specimen groups classification

Specimen ID	GNP wt%	GNP Type	Width × Length (mm × mm)
Baseline	0	---	100 × 100
0.5 wt%-PG	0.5	PG	100 × 100
1 wt%-PG	1	PG	100 × 100
2 wt%-PG	2	PG	100 × 100
0.5 wt%-NH2-G	0.5	NH2-G	100 × 100
1 wt%-NH2-G	1	NH2-G	100 × 100
2 wt%-NH2-G	2	NH2-G	100 × 100

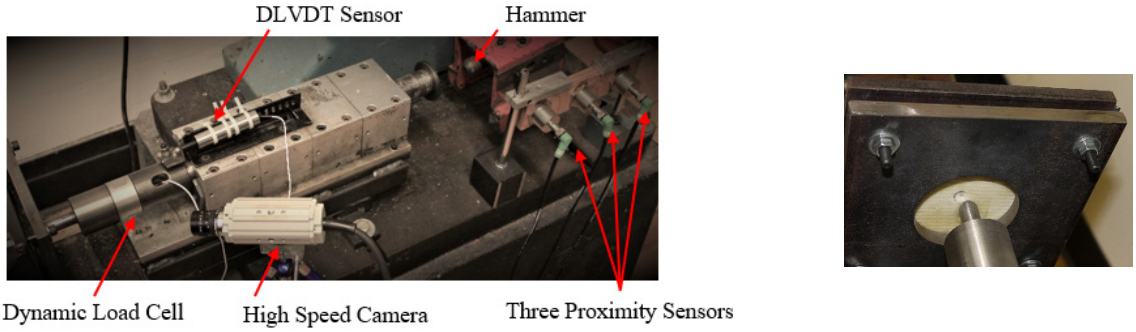

(a) (b)

Figure 3. (a) The Impact test equipment, (b) The fixture used to hold the specimen

Three proximity sensors were mounted at a set distance apart along the travel path of the impacting mass. Each sensor emitted a signal once the mass passed across it. A dynamic load cell and a dynamic linear variable differential transformer sensor (DLVDT) were also used to measure the impact load and displacement, respectively. The signals of proximity sensors, DLVDT and dynamic load cell were all captured through a DAQ-board, controlled by the LabVIEW software. The response of each specimen was captured by recording the impact contact force and signals obtained through the proximity sensors, and the resulting displacement measured at centre location of each impacted specimen. The impact energy was then calculated based on the impact mass and swing angle of the pendulum. In addition, the impact velocity was obtained from the proximity sensors' signals.

4. Results and Discussions

4.1. Load- and Displacement-Time Histories

As mentioned earlier, a total of 63 specimens were tested under three different impact energy levels. Figure 4 illustrates the force- and displacement-time histories of all seven groups of specimens subjected to three different energy levels. As can be seen, the impact force-time history curve of each group of specimens (i.e., regardless of GNP type and wt% content) essentially plateaus at almost the same magnitude of force. The variation of the load-history curves before attaining their peak values is quasi-linear. The slope of this portion of the curves (which is referred to as the "contact stiffness" [27]) is lower for the baseline specimens; however, the slopes of the curves of specimens reinforced with PG or NH2-G are quite similar, regardless of wt% GNP content. At relatively low impact energies (i.e., the energy levels that caused no perforation), the contact stiffness varies quasi-linearly until a damage develops on the impacted surface of the specimens. An abrupt change in the curve signifies the development of a crack on the impacted surface. After this stage, the impactor bounces back, and the force decreases to zero. At the higher impact energy level (i.e. energy levels causing perforation), the force increases with an almost linear variation with respect to time, but with a high rate, and then decreases abruptly once the impactor perforates the specimens. The sharp decrease in the load, as opposed to sudden decrease of it to zero, is due to the friction between the impactor's body and perforation boundary.

In the case of baseline specimens, the impactor partially perforated through the specimens and caused a crack on the non-impacted surface, followed by bouncing-back of the impactor. The response can also be depicted through examination of the load- and displacement-time history curves. The force-time history curves of the PG and NH2-G specimens impacted at impact energy of 40J are quite similar,

signifying that the impactor did not perforate into the specimens, but generated a crack or permanent deformation on the impacted surface. This is also confirmed by the variations seen in the displacement-time history curves, which indicates that the impactor generated a crack and bounced back without perforating the specimens. The force-time history curves of PG specimens, subjected to 40 J impact energy attained their maximum values almost at the same magnitude; nevertheless, specimens with 1 wt%-PG exhibited the longest contact duration. In the case of NH2-G group of specimens, the maximum contact force increased by 27% and 14% in 1 wt%-NH2-G and 2 wt%-NH2-G specimens, respectively, in comparison to the baseline specimens. Moreover, the contact time of these two groups of specimens increased by 35% and 48% respectively.

Moreover, the comparison of displacement-time history curves of both PG and NH2-G groups of specimens reveals that inclusion of GNP enabled the specimens to undergo more deformations (by a maximum of 46% for 1 wt%-NH2-G and 91% for 1 wt%-PG) prior to stress-softening. It should be noted that inherently, 3DFMLs respond to impact load in a ductile manner. The comparatively larger observed deformation response implies improved ductility of their response. This observation, concludes that, at 40 J impact energy, inclusion of 1 wt% of PG and NH2-G nanoparticles offers the greatest improvement in the ductile response of 3DFML panels.

The time histories of all four groups of specimens, subjected to 50 J impact energy is also illustrated in Figure 4. Examination of the displacement-time history curves would reveal that the PG group of specimens experienced perforation when subjected to 50 J energy, while specimens with 0.5 wt% and 1 wt% GNP content resisted perforation. In contrast, the time history curves of specimens with 2 wt%-PG content and baseline specimen evidence through-thickness perforation of specimens by the impactor. The maximum contact forces observed for the baseline and 1 wt%-PG specimens are comparable; however, the contact force decreased in specimens with 0.5 wt%-PG and 2 wt%-PG contents. In fact, the 0.5 wt% and 1 wt%-NH2-G specimens that were subjected to 50 J impact energy experienced a sequence of cracking, but no perforation. Specifically, crack developed on the impacted surface of specimens with 0.5 wt% NH2-G, while another crack developed on the other surface of the specimens that contained 1 wt%-NH2-G. The first decrease in the force history curves of these specimens is associated with the creation of the first crack. As seen, the load capacity increases after this stage, followed by a subsequent abrupt decrease in load capacity, indicating the development of a crack on the non-impacted surface. The maximum contact force increased by 22% in specimens with 1 wt%-NH2-G in comparison to the contact force of baseline specimens. The shape of the force history curve and larger displacement endured by specimens with 2 wt%-NH2-G indicates the perforation of those specimens when subjected to 50 J impact energy. Moreover, the ductile response observed in the specimens under 40 J impact event was also observed at 50 J event for both PG and NH2-G specimens. Moreover, specimens with NH2-G and PG contents endured approximately 30% and 84% more displacement, respectively, compared to the baseline specimens.

In the 60 J impact events, the impactor penetrated into all baseline and nano-reinforced specimens. However, specimens with 2 wt% PG content endured a larger deformation and lower contact force in comparison to the baseline specimens. The maximum contact force experienced by 0.5 wt% and 1 wt% PG and 0.5 wt% and 2 wt% NH2-G specimens are almost identical to that sustained by the baseline specimens. However, examination of the last portion of the displacement-time history curves of specimens with 1 wt% PG and NH2-G content indicates that the impactor bounced back and did not thoroughly penetrate through the specimens. It can be therefore concluded that 3DFMLs with 1wt% PG and NH2-G contents showed greater perforation tolerance.

4.2. Force-Displacement Response

In this section, specimens' behaviours are compared based on their force-displacement response, as illustrated in Figure 5. The initial slope of force-displacement curves represents the 'impact bending stiffness' of specimens [23]. It can be observed that under impact energy levels that did not result in a through-penetration, the addition of PG and NH2-G particles could not improve the impact bending stiffness of the 3DFMLs. The force-displacement graphs of GNP-based specimens indicate that the impactor rebounded after the initial impact. Moreover, the bending stiffness of specimens reinforced with PG and NH2-G are almost identical, but considerably larger than those exhibited by the baseline specimens. As can be seen from the results shown in Figure 5(c), when specimens were impacted at 70 J energy, all specimens, with the expectation of those with 1 wt% PG and NH2-G contents were perforated.

4.3. Damage Mechanism

Figure 6 illustrates the damage mechanisms of all seven groups of specimens subjected to the three different levels of impact energy. The damaged area of the impacted specimen is measured using a Dino-Lite digital microscope and its accompanying DinoCapture software. Figure 6 illustrates the post-test pictures of all groups of specimens tested at all three different impact energies. As seen from the results summarized in Figure 7, the damage area increased as impact energy was increased. Note that the variation in the damaged area in the non-impacted surface is greater than that observed on the impacted surface. The damage areas on the impacted and non-impacted surfaces of the baseline group of specimens impacted at 70 J energy increased by 32% and 416%, respectively, in comparison to those that were subjected to 40 J impact energy. This trend is also observed for the cases of PG and NH2-G groups of specimens.

It is believed that inclusion of the GNPs improves the impact response of 3DFMLs by enhancing the fracture

toughness of the resin used to bond the Mg layers to the 3D fiber-glass fabric core. This is emerged through the phenomenon known as crack bridge mechanism. Additionally, the functionalization of GNP further enhances the fracture toughness by improving the interfacial strength between GNPs and epoxy.

The mechanism of crack-bridging can be clearly seen in the SEM image produced in one of our earlier works, as shown in Figure 9 [36]. The evidence of some GNP particles that have been pulled out of one side of the fracture surface (see the white arrows) is quite clear in the image, indicating bridging of the crack surfaces. It should be noted that one of the important attributes of GNP particles is their jagged boundary curvatures, which provides added resistance against the pull-out forces to an advancing crack. In other words, the "mechanical locking" resistance is enhanced by addition of GNPs. Moreover, since damage created by an impact results in a mixed mode fracture, the surface roughness induced by GNP particles would further enhance the resistance of the interface against advancing mode II fracture. Therefore, in theory, the more is the GNP wt% content, the larger would be the force required to pull-out the GNP particles; as a result, increasing the fracture energy required for crack propagation. However, the caveat is that in practice, increase in GNP content beyond a certain level, would cause agglomeration of the GNPs, thus leading to creation of stress concentration, which in turn would reduce the fracture resistance at the interface.

Comparison of damage regions in specimens subjected to impact energy of 40 J reveals that the extent of damage to the baseline specimens is significantly greater than the GNP-based specimens. The damaged area of impacted surface of PG and NH2-G groups respectively decreased by maximum 41% and 42%, respectively, in comparison to the baseline group. Moreover, damage areas in both impacted and non-impacted surfaces are smaller in the NH2-G specimens in comparison with the PG specimens. In average, damage areas on the non-impacted surface of NH2-G specimens are 72% lower than those of the baseline specimens.

The presented results for energy levels of 50 J indicate that the extent of damage on both impacted and non-impacted surfaces was the lowest in specimens containing NH2-G. The measured damaged areas in the specimens with 1 wt% NH2-G were 45% and 67% (on the impacted and non-impacted surface, respectively) were lower than those observed for the baseline specimens.

Similar to the results discussed for the previous energy levels, the extent of perforation areas was also lower in specimens with NH2-G content in comparison to those with PG content and baseline specimens. The results indicate that addition of either 0.5 wt% or 1 wt% NH2-G nanoparticles would minimize the extent of damage in the 3DFMls when subjected to such impact loadings.

4.4. Global Features of GNP-3DFML

As stated earlier, the main objective of present study has been the establishment of the effects of GNP nanoparticles on the impact response of a recently developed 3DFML. In this section, the global effect of addition of PG and NH2-G particles to the resin is summarized, and the optimal %wt of GNP content that could produce the maximum enhancement in 3DFML's impact response is established.

As discussed earlier, inclusion of PG in the resin did not produce any enhancement in the impact force endurance of the 3DFMLs. However, the inclusion increased the contact stiffness of 3DFMLs. Although, the inclusion of NH2-G improved impact force capacity of all specimens, regardless of wt% content, the most notable enhancement of 31% in the contact force was observed for the specimens with 1 wt% NH2-G content. Furthermore, inclusion of both PG and NH2-G nanoparticles increased the maximum local deformation that the specimens could sustain under all the applied impact energy levels. The corresponding results are presented and compared for all groups of specimens in Figure 8 (a) and (b). Moreover, the variation in the energy restitution coefficient (ERC) (a parameter that is a function of the absorbed impact energy [38]) as a function of GNP type and weight content is also illustrated in Figure 8 (c). The results indicate that specimens with NH2-G content exhibited the greatest levels of energy-absorption capacity among all groups of specimens. The ERC of specimens containing 1 wt% NH2-G (measured at the perforation level of impact energy), is greater by 80% and 89%, respectively, when compared to those of the baseline and 1 wt% PG-content specimens. Note that a lower value of ERC would indicate higher energy absorption capacity; therefore, specimens containing 1 wt% NH2-G exhibited the largest energy absorption capacity among all groups of specimens. On the other hand, when the %wt content of PG and NH2-G was increased to 2 wt%, degrading effects in both the impact capacity and damage area were observed. These degradations are attributed to the agglomeration of GNP particles, which results due to nonuniform dispersion of the particles when the content surpasses a certain value [31].

In summary, the collective results indicate that the addition of 0.5 wt% and 1 wt% PG and NH2-G nanoparticles within the resin used to mate the 3DFGF to MgA sheets would improve the ductility, deformability and energy-absorption capacity of the 3DFML. However, according to the experimental results, the optimal response could be attained at 1 wt% NH2-G content.

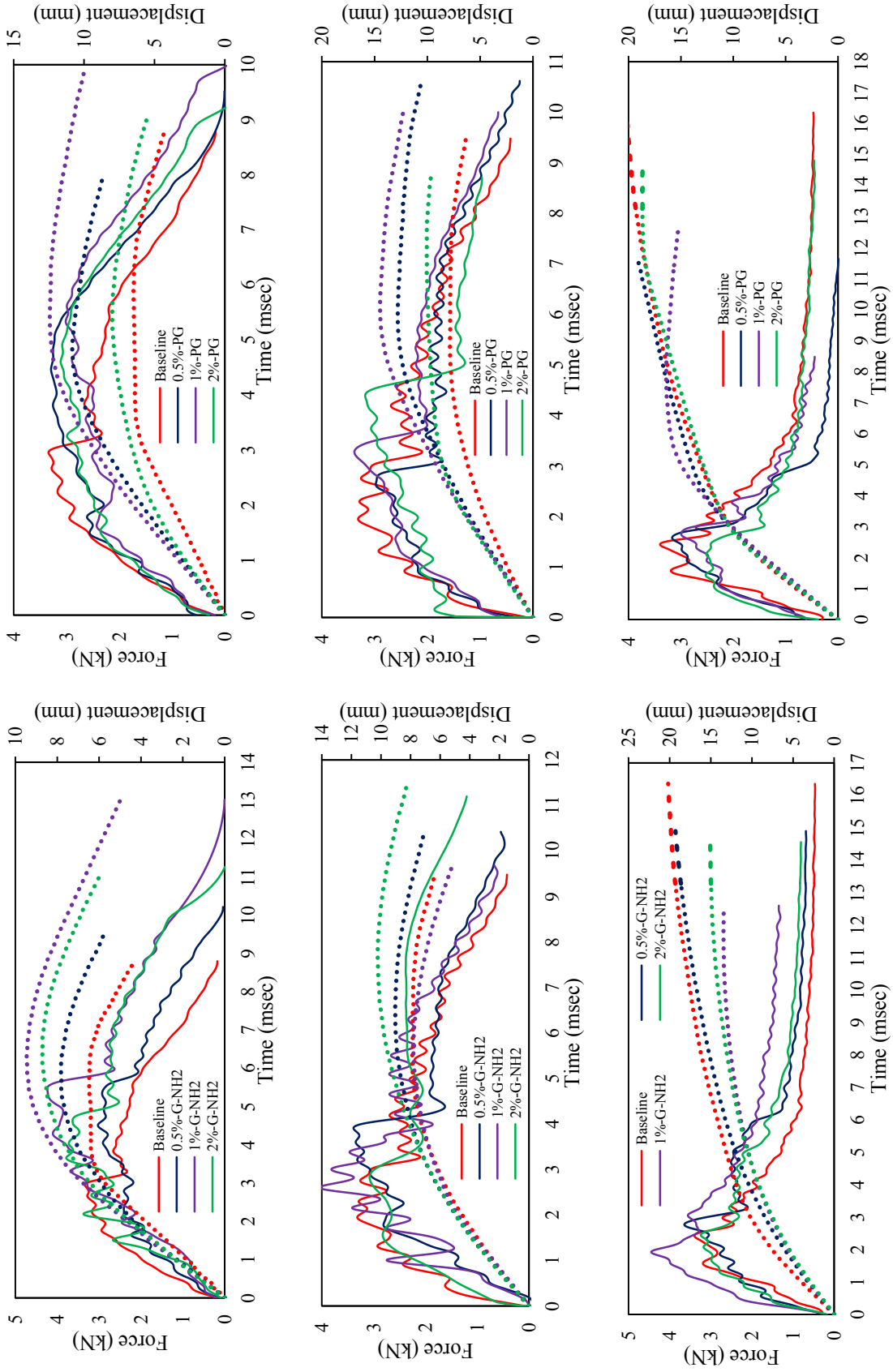

Figure 4. Force- and displacement-time history responses of all specimen groups impacted at energy levels of 40 J (1st row), 50 J (2nd row) and 70 J (3rd row)

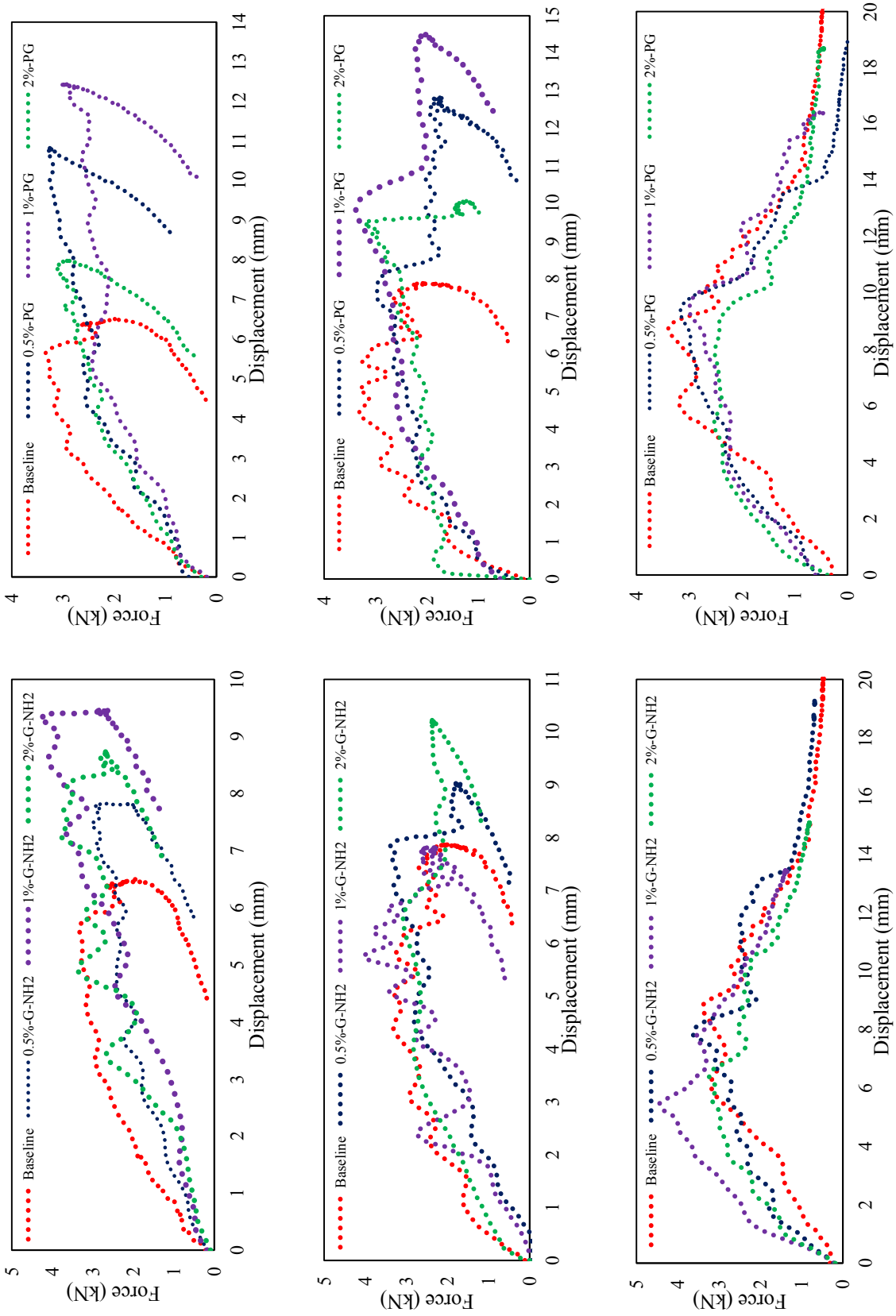

Figure 5. Force-displacement curves of all specimen groups impacted at energy levels of 40 J (1st row), 50 J (2nd row) and 70 J (3rd row)

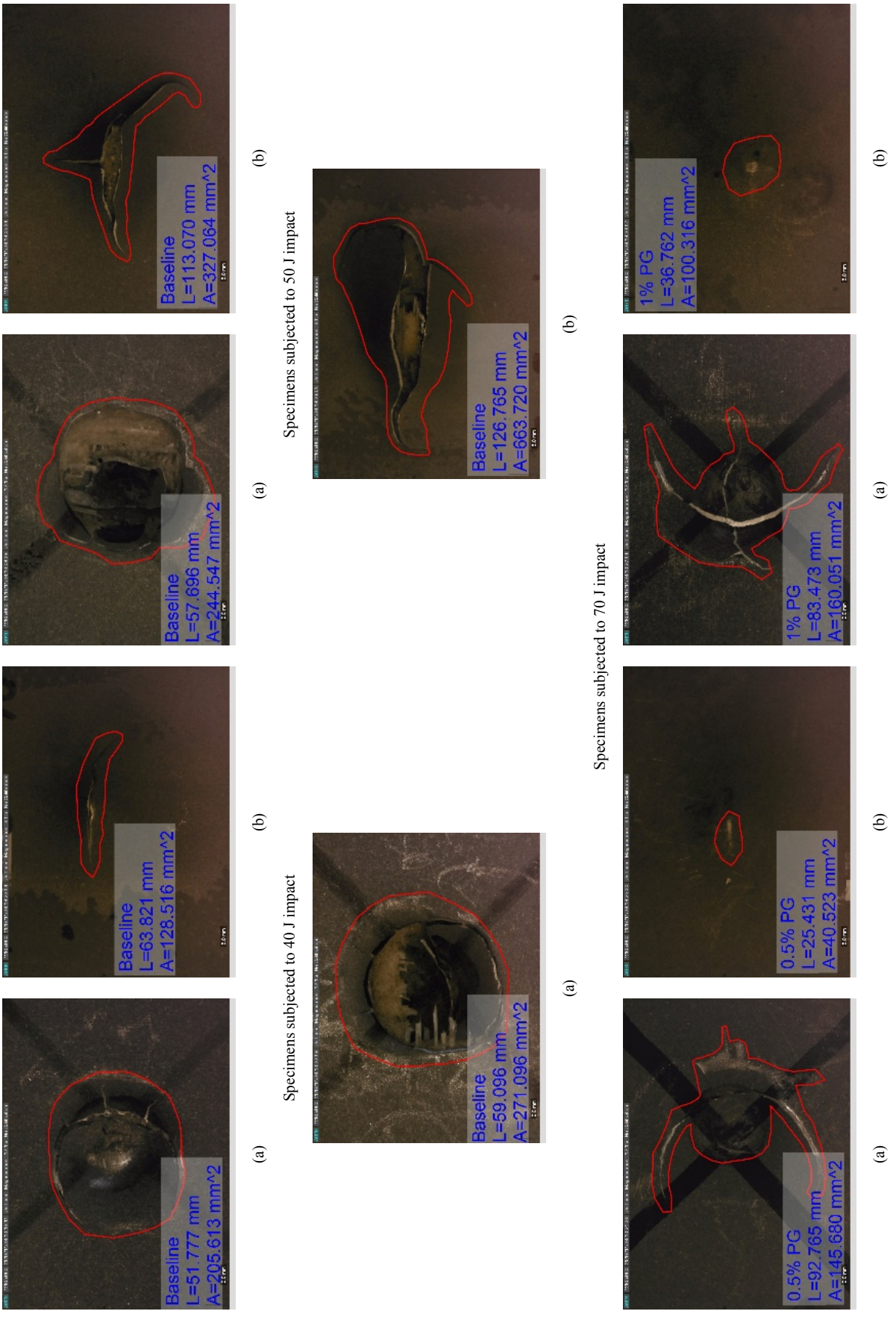
Baseline
L=51.777 mm
A=205.613 mm^2
Baseline
L=63.821 mm
A=128.516 mm^2
Baseline
L=57.696 mm
A=244.547 mm^2
Baseline
L=113.070 mm
A=327.064 mm^2
Specimens subjected to 40 J impact
Baseline
L=59.096 mm
A=271.096 mm^2
Baseline
L=126.765 mm
A=663.720 mm^2
Specimens subjected to 50 J impact
0.5% PG
L=92.765 mm
A=145.680 mm^2
0.5% PG
L=25.431 mm
A=40.523 mm^2
1% PG
L=83.473 mm
A=160.051 mm^2
1% PG
L=36.762 mm
A=100.316 mm^2
Specimens subjected to 70 J impact
(a)
(b)

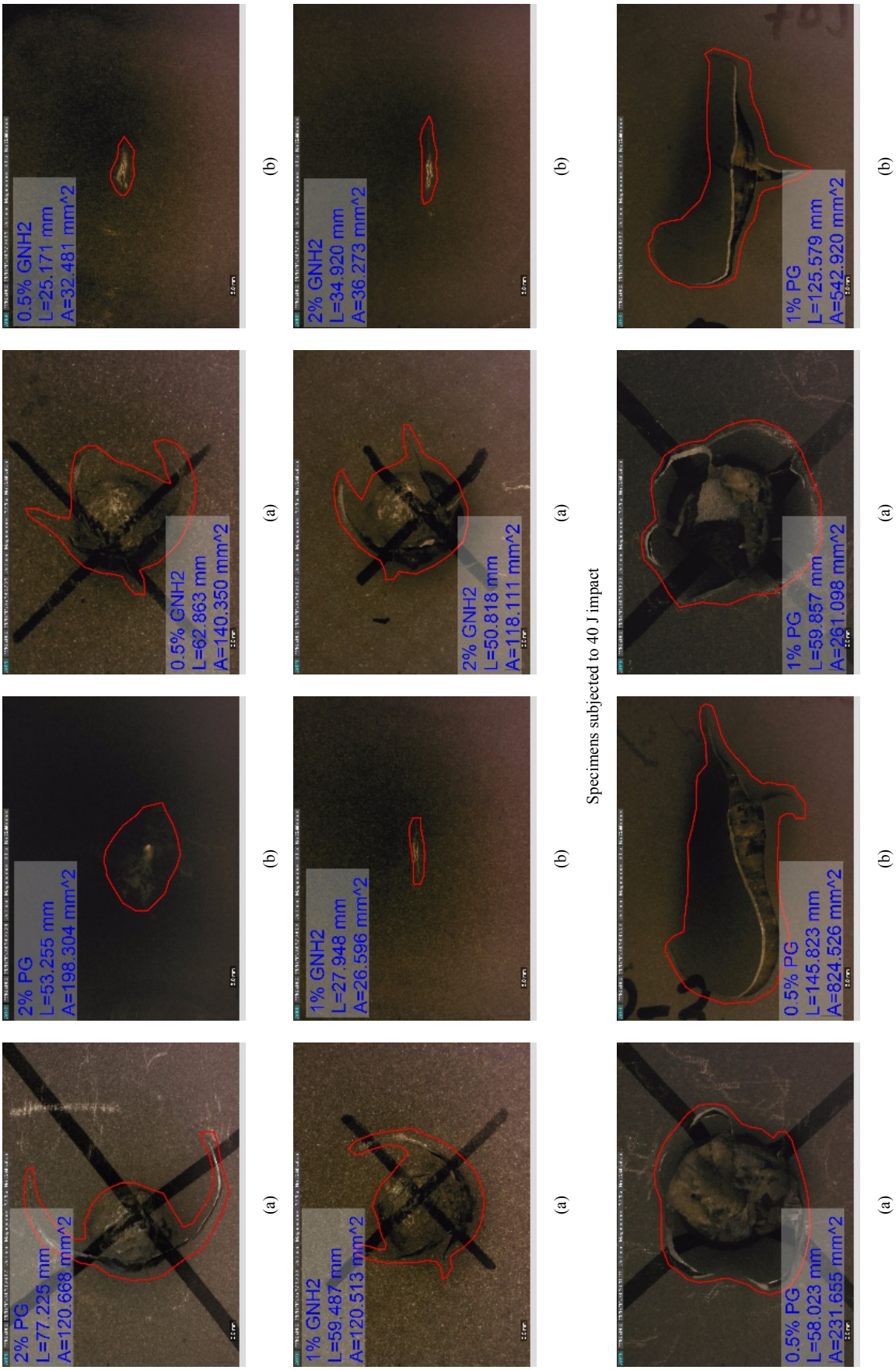

Specimens subjected to 40 J impact

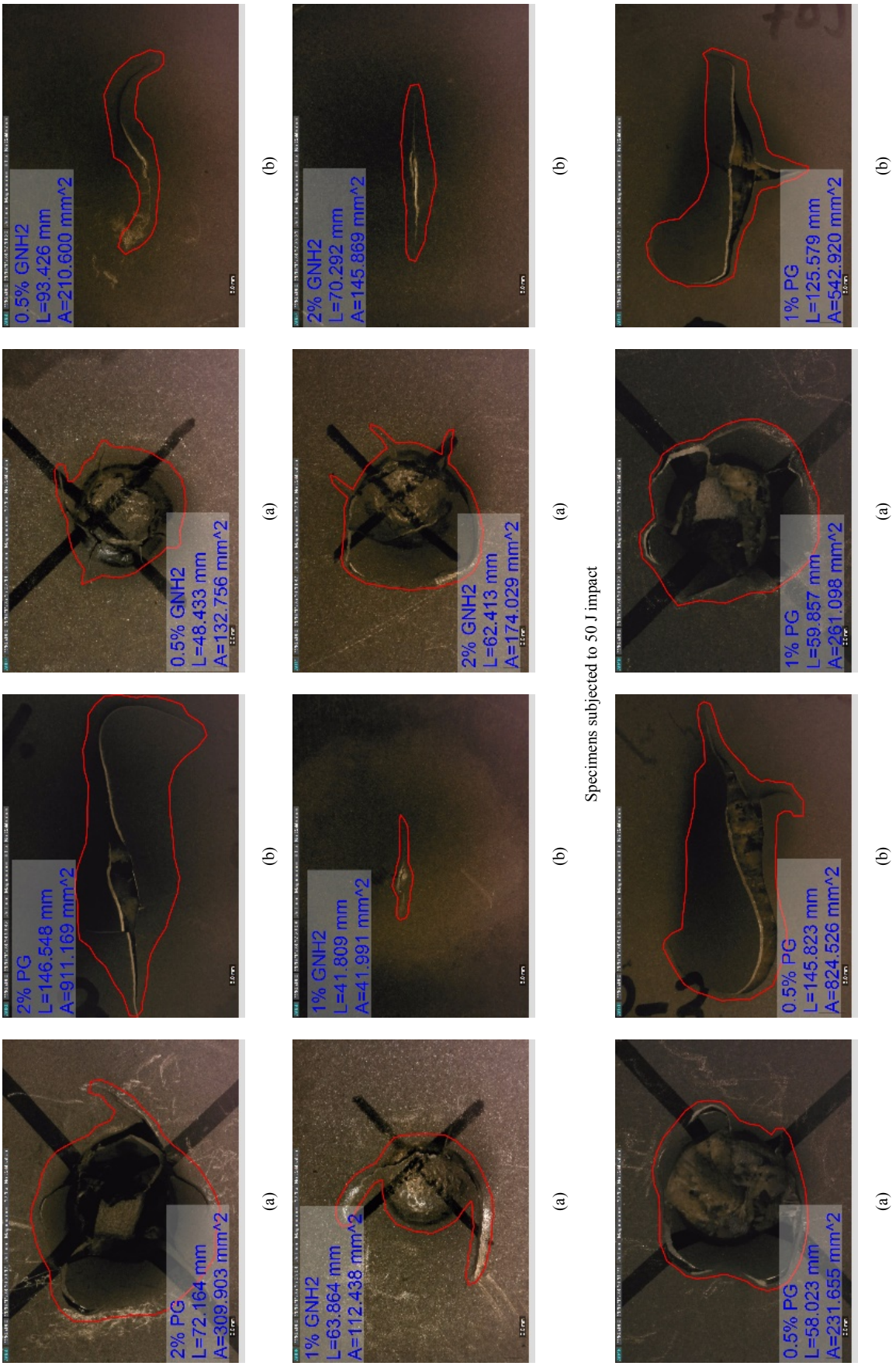
0.5% GNH2
L=93.426 mm
A=210.600 mm^2
(b)
0.5% GNH2
L=48.433 mm
A=132.756 mm^2
(a)
2% PG
L=146.548 mm
A=911.169 mm^2
(b)
2% PG
L=72.164 mm
A=309.903 mm^2
(a)
2% GNH2
L=70.292 mm
A=145.869 mm^2
(b)
2% GNH2
L=62.413 mm
A=174.029 mm^2
(a)
1% GNH2
L=41.809 mm
A=41.991 mm^2
(b)
1% GNH2
L=63.864 mm
A=112.438 mm^2
(a)
1% PG
L=125.579 mm
A=542.920 mm^2
(b)
1% PG
L=59.857 mm
A=261.098 mm^2
(a)
0.5% PG
L=145.823 mm
A=824.526 mm^2
(b)
0.5% PG
L=58.023 mm
A=231.655 mm^2
(a)
Specimens subjected to 50 J impact

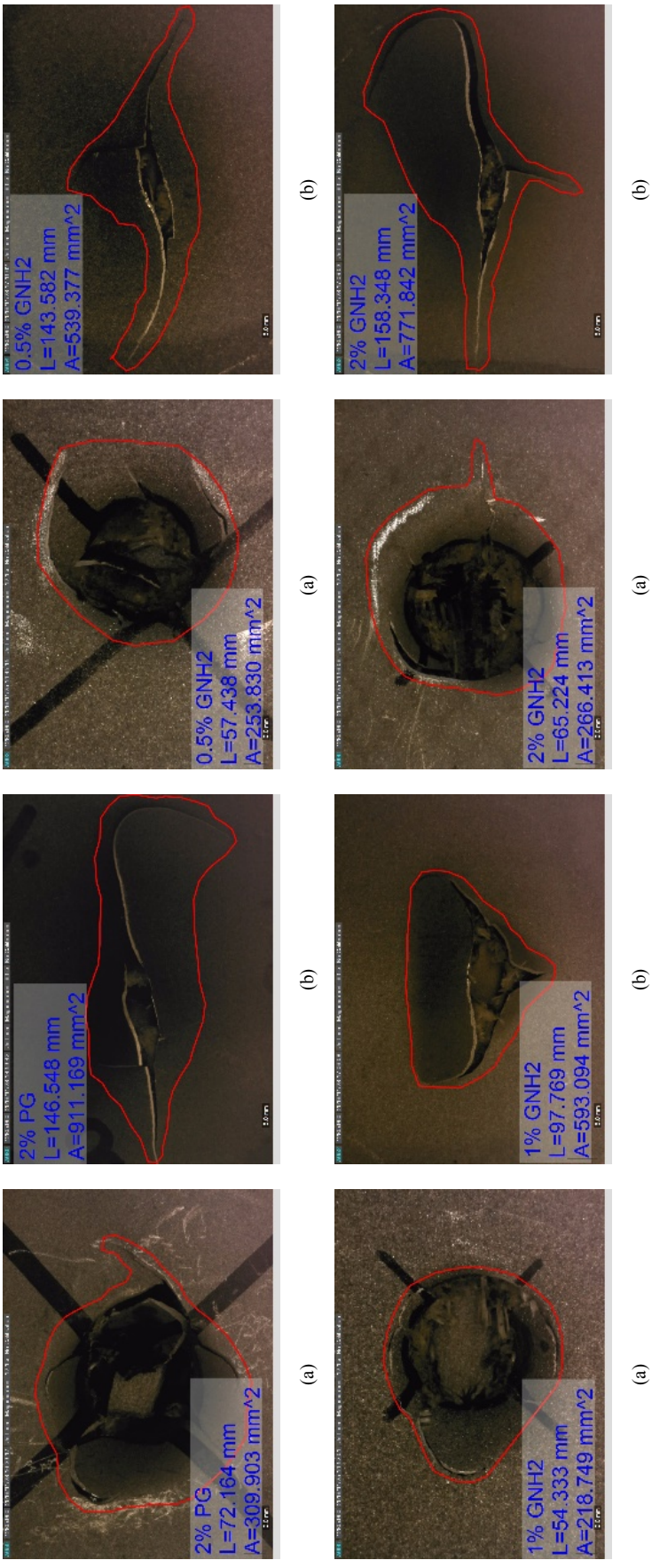

Specimens subjected to 70 J impact

Figure 6. Damage mechanisms of all groups of specimens (a) on the impacted surface and (b) on non-impacted surface

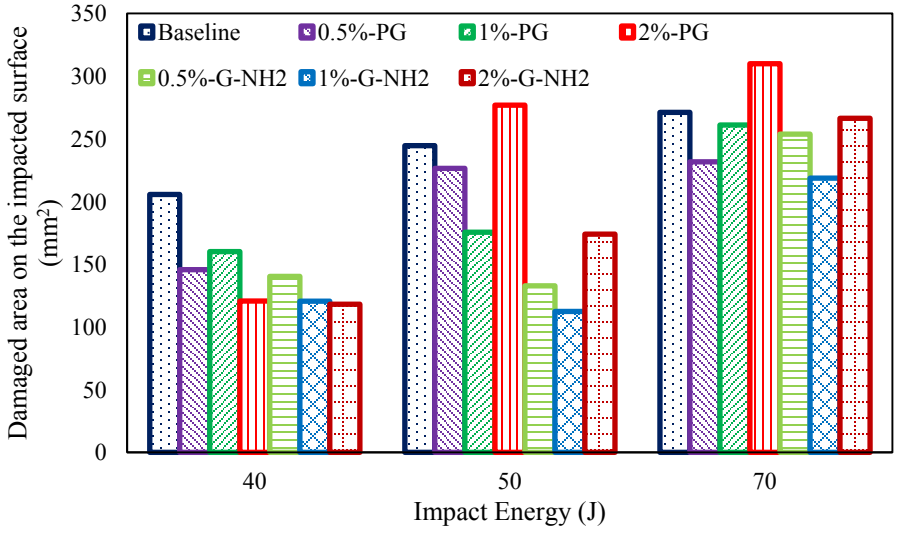

(a)

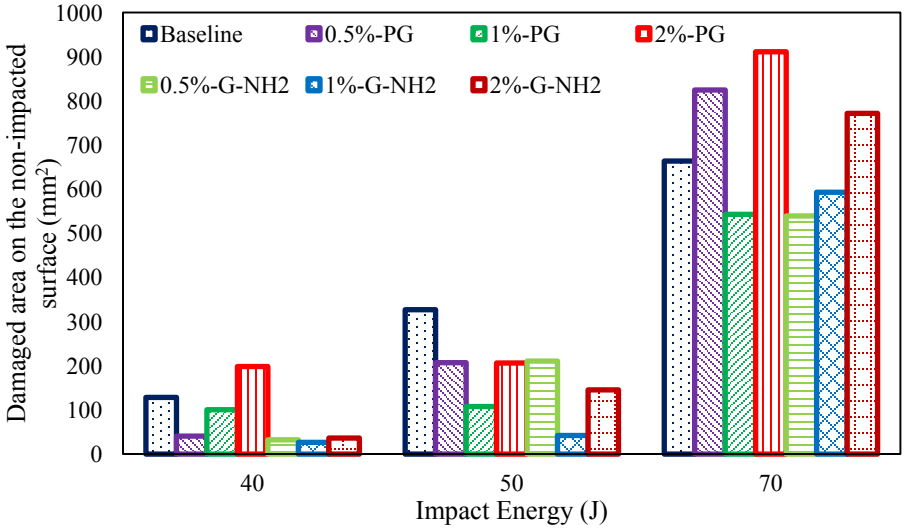

(b)

Figure 7. Damaged area of impacted specimens on the (a) impacted surface, and (b) non-impacted surface

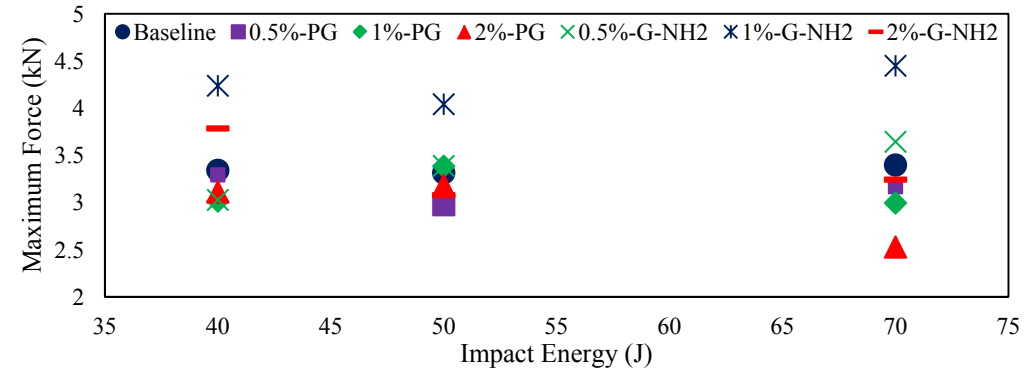

(a)

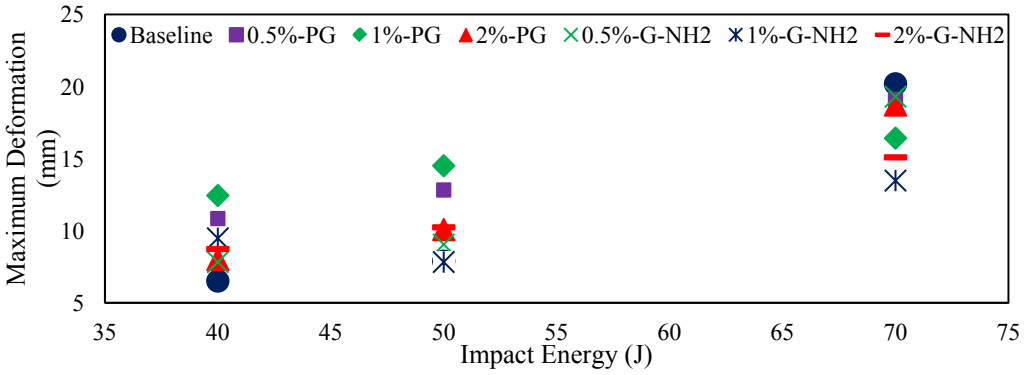

(b)

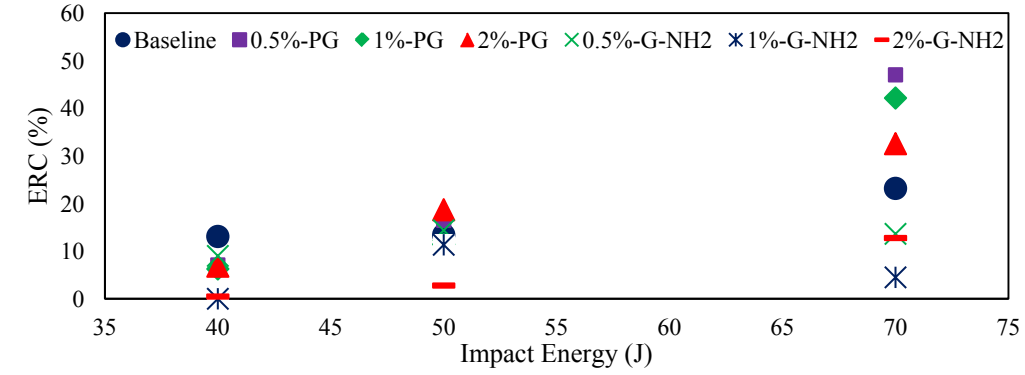

(c)

Figure 8. Variation in (a) maximum force, (b) maximum deformation and (c) ERC as a function of GNP type and weight-content for the seven groups of specimens subjected to three different impact energy levels

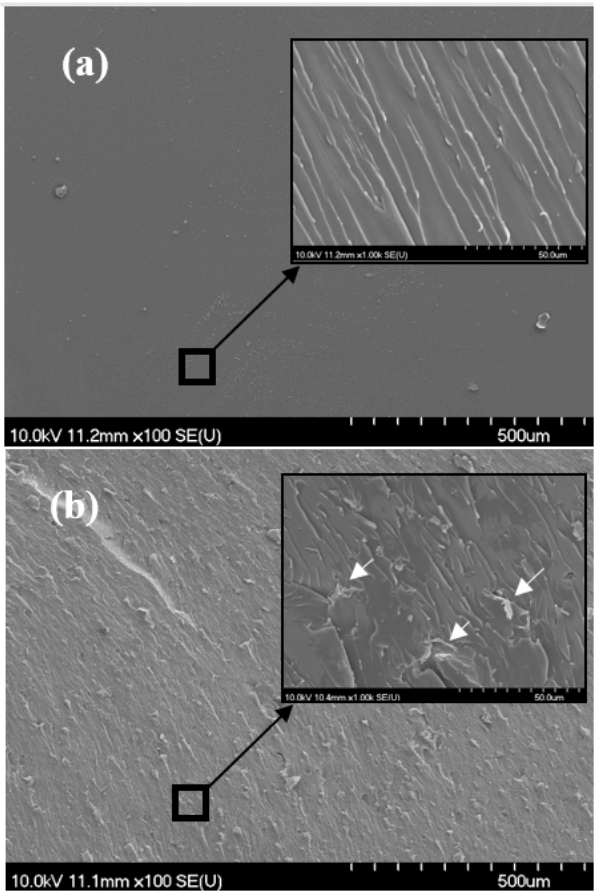

Figure 9. Fracture surfaces of the resin reinforced with and without GNP particles; (a) neat resin, (b) 0.5 wt% [39]

5. Summary and Conclusions

The main objective of this study was to investigate whether the inclusion of graphene nanoplatelets (GNP), a relatively inexpensive nanocarbon particles, in the resin used to mate the constituents of a novel 3D fiber-metal laminate (3DFML), could enhance the performance of such FMLs under low-velocity impact loading state. Two different types GNPs, with four different wt% (weight percentage) GNP contents were considered (i.e., 0, 0.5, 1 and 2 wt%), so that the optimal GNP content could be established. In total, 63 3DFML specimens were fabricated and tested under three impact energies.

The results revealed that specimens with resin containing amino-functionalized GNP particles (NH2-G) exhibited improved impact response in comparison to those containing pristine GNP (PG) or with no nanoparticles (i.e., neat epoxy). It was observed that the addition of 0.5 wt% and 1 wt% of PG and NH2-G to resin improved the ductility of 3DFMLs. Moreover, 3DFMLs with 0.5 wt% and 1 wt% GNP contents could sustain larger local displacement (hence were more resilient) than the baseline specimens and those with 2 wt% GNP content in the tests in which the energy levels were less than that causing perforation. In all, the 3DFMLs containing NH2-G showed better performance and energy-absorption capacity among all groups of specimens. Furthermore, this group also sustained less damage (i.e., in terms of the extent of damage areas developed on specimens' surfaces, as well as the extent of through-thickness damage).

The results also conclusively indicate that the optimal GNP content would be 1 wt%. When GNP content was increased to 2 wt%, the ductility and energy-absorption capacity of the 3DFML specimens were degraded in comparison to the baseline and specimens containing either 0.5 or 1 wt% GNP contents. This degradation is believed to be due to the agglomeration of GNP particles, causing non-uniform dispersion of the nanoparticles within the resin.

ACKNOWLEDGEMENTS

This financial support received through the National Science and Engineering Research Council of Canada (NSERC) in support of this study is gratefully appreciated. The Killam scholarship awarded to the first author is also gratefully acknowledged.

REFERENCES

[1] Ltd. CBFC. 3D fiberglass fabric manual. China Beihai Fiberglass Co Ltd. 2016.

[2] Sadighi M, Alderliesten R, Benedictus R. Impact resistance of fiber-metal laminates: a review. International Journal of Impact Engineering. 2012; 49:77-90.

[3] Vermeeren C. An historic overview of the development of fibre metal laminates. Applied Composite Materials. 2003; 10(4-5): 189-205.

[4] Gunnink J, Vlot A, Alderliesten R, van der Hoeven W, de Boer A, Sinke J, et al. Towards technology readiness of fibre metal laminates. GLARE Technology development (GTO), ICAS 2000 CONGRESS2000.

[5] Marissen R. Mechanical aspects related to fibre fracture in ARALL® 2 laminates. Advances in Fatigue Science and Technology: Springer; 1989. p. 697-707.

[6] Vlot A, Gunnink J. Fibre Metal Laminatese - an introduction. Dordrecht, The Netherlands: Kluwer Academic Publisher. 2001.

[7] Feng D, Aymerich F. Damage prediction in composite sandwich panels subjected to low-velocity impact. Composites Part A: Applied Science and Manufacturing. 2013; 52: 12-22.

[8] Tooski MY, Alderliesten R, Ghajar R, Khalili S. Experimental investigation on distance effects in repeated low velocity impact on fiber–metal laminates. Composite Structures. 2013; 99: 31-40.

[9] Morinière F, Alderliesten R, Sadighi M, Benedictus R. An integrated study on the low-velocity impact response of the GLARE fibre-metal laminate. Composite Structures. 2013; 100: 89-103.

[10] Feng D, Aymerich F. Finite element modelling of damage induced by low-velocity impact on composite laminates. Composite Structures. 2014; 108: 161-71.

[11] Payeganeh G, Ghasemi FA, Malekzadeh K. Dynamic response of fiber–metal laminates (FMLs) subjected to low-velocity impact. Thin-Walled Structures. 2010; 48(1): 62-70.

[12] Zhou J, Hassan MZ, Guan Z, Cantwell WJ. The low velocity impact response of foam-based sandwich panels. Composites science and Technology. 2012; 72(14):1781-90.

[13] Tan C, Akil HM. Impact response of fiber metal laminate sandwich composite structure with polypropylene honeycomb core. Composites Part B: Engineering. 2012; 43(3): 1433-8.

[14] Sadighi M, Pärnänen T, Alderliesten R, Sayeaftabi M, Benedictus R. Experimental and numerical investigation of metal type and thickness effects on the impact resistance of fiber metal laminates. Applied Composite Materials. 2012; 19(3-4): 545-59.

[15] Tsartsaris N, Meo M, Dolce F, Polimeno U, Guida M, Marulo F. Low-velocity impact behavior of fiber metal laminates. Journal of Composite Materials. 2011:0021998310376108.

[16] Fan J, Cantwell W, Guan Z. The low-velocity impact response of fiber-metal laminates. Journal of Reinforced Plastics and Composites. 2011; 30(1): 26-35.

[17] Yaghoubi AS, Liu Y, Liaw B. Stacking sequence and geometrical effects on low-velocity impact behaviors of GLARE 5 (3/2) fiber–metal laminates. Journal of thermoplastic composite materials. 2012; 25(2): 223-47.

[18] Zhu S, Chai G. Low-velocity impact response of fiber-metal laminates–A theoretical approach. Proceedings of the Institution of Mechanical Engineers, Part L: Journal of Materials Design and Applications. 2013: 1464420713489616.

[19] Vlot A, Alderliesten R, Hooijmeijer P, Kanter Jd, Sinke J, Ypma M. Fibre metal laminates: a state of the art. International Journal of Materials and Product Technology. 2002; 17(1-2): 79-98.

[20] Morinière F, Alderliesten R, Benedictus R. Modelling of impact damage and dynamics in fibre-metal laminates–a review. International Journal of Impact Engineering. 2014; 67: 27-38.

[21] Starikov R. Assessment of impact response of fiber metal laminates. International Journal of Impact Engineering. 2013; 59: 38-45.

[22] Vlot A. Impact loading on fibre metal laminates. International Journal of Impact Engineering. 1996; 18(3): 291-307.

[23] Taraghi I, Fereidoon A, Taheri-Behrooz F. Low-velocity impact response of woven Kevlar/epoxy laminated composites reinforced with multi-walled carbon nanotubes at ambient and low temperatures. Materials & Design. 2014; 53: 152-8.

[24] Avila AF, Soares MI, Neto AS. A study on nanostructured laminated plates behavior under low-velocity impact loadings. International journal of impact engineering. 2007; 34(1): 28-41.

[25] Balaganesan G, Velmurugan R, Kanny K. Dynamic Response of Nanocomposite Laminates During Low, Medium and High Velocity Impact Loading. Frontiers in Aerospace Engineering. 2015.

[26] Haq M, Umer R, Khomenko A, Loos A, Drzal L. Manufacturing and impact behavior of sandwich composites with embedded graphene platelets. The 19th International Conference on Composite Materials, Montreal, Canada July 28-August 2013.

[27] Hosur MV, Chowdhury F, Jeelani S. Low-velocity impact response and ultrasonic NDE of woven carbon/epoxy — Nanoclay nanocomposites. Journal of Composite Materials. 2007; 41(18): 2195-212.

[28] Ulus H, Üstün T, Şahin ÖS, Karabulut SE, Eskizeybek V, Avcı A. Low-velocity impact behavior of carbon fiber/epoxy multiscale hybrid nanocomposites reinforced with multiwalled carbon nanotubes and boron nitride nanoplates. Journal of Composite Materials. 2015:0021998315580835.

[29] Ávila AF, Carvalho MGR, Dias EC, da Cruz DTL. Nano-structured sandwich composites response to low-velocity impact. Composite Structures. 2010; 92(3): 745-51.

[30] Soliman EM, Sheyka MP, Taha MR. Low-velocity impact of thin woven carbon fabric composites incorporating multi-walled carbon nanotubes. International Journal of Impact Engineering. 2012; 47: 39-47.

[31] Lin J-C, Chang L, Nien M, Ho H. Mechanical behavior of various nanoparticle filled composites at low-velocity impact. Composite Structures. 2006; 74(1): 30-6.

[32] Asaee Z, Shadlou S, Taheri F. Low-velocity impact response of fiberglass/magnesium FMLs with a new 3D fiberglass fabric. Composite Structures. 2015; 122: 155-65.

[33] Asaee Z, Taheri F. Characterization of the Mechanical and Impact Response of a New-Generation 3D Fiberglass Fabric. American Society of Composites-30th Technical Conference 2015.

[34] Asaee Z, Taheri F. Experimental and numerical investigation into the influence of stacking sequence on the low-velocity impact response of new 3D FMLs. Composite Structures. 2016; 140: 136-46.

[35] Asaee Z, Mohamed M, Soumik S, Taheri F. Experimental and numerical characterization of delamination buckling behavior of a new class of GNP-reinforced 3D fiber-metal laminates. Thin-Walled Structures. 2017; 112: 208-16.

[36] Ahmadi-Moghadam B, Sharafimasooleh M, Shadlou S, Taheri F. Effect of functionalization of graphene nanoplatelets on the mechanical response of graphene/epoxy composites. Materials & Design. 2015; 66: 142-9.

[37] Ahmadi-Moghadam B, Taheri F. Effect of processing parameters on the structure and multi-functional performance of epoxy/GNP-nanocomposites. Journal of Materials Science. 2014; 49(18):6180-90.

[38] Sadighi M, Pärnänen T, Alderliesten RC, Sayeaftabi M, Benedictus R. Experimental and Numerical Investigation of Metal Type and Thickness Effects on the Impact Resistance of Fiber Metal Laminates. Applied Composite Materials. 2012; 19(3): 545-59.

[39] Ahmadi-Moghadam B, Taheri F. Fracture and toughening mechanisms of GNP-based nanocomposites in modes I and II fracture. Engineering Fracture Mechanics. 2014; 131: 329-39.